Improving malignancy prediction in breast lesions with the combination of apparent diffusion coefficient and dynamic contrast-enhanced kinetic descriptors

Luisa Nogueira [a,b,*], Sofia Brandão [c], Eduarda Matos [d], Rita Gouveia Nunes [e], Hugo Alexandre Ferreira [e], Joana Loureiro [c], Isabel Ramos [b]

[a] *Department of Radiology, School of Health Technology of Porto/Polytechnic Institute of Porto (ESTSP/IPP), Rua Valente Perfeito, 4400-330 Vila Nova de Gaia, Portugal*
[b] *Department of Radiology, Hospital de São João/Faculty of Medicine of Porto University (FMUP), Alameda Prof. Hernani Monteiro, 4200-319 Porto, Portugal*
[c] *MRI Unit, Department of Radiology, Hospital de São João, Alameda Prof. Hernani Monteiro, 4200-319 Porto, Portugal*
[d] *Department of Health Community, Institute of Biomedical Sciences Abel Salazar of Porto University (ICBAS), Porto, Portugal*
[e] *Institute of Biophysics and Biomedical Engineering (IBEB), Faculty of Sciences, University of Lisbon, Campo Grande, 1749-016 Lisboa, Portugal*

AIM: To assess how the joint use of apparent diffusion coefficient (ADC) and kinetic parameters (uptake phase and delayed enhancement characteristics) from dynamic contrast-enhanced (DCE) can boost the ability to predict breast lesion malignancy.

MATERIALS AND METHODS: Breast magnetic resonance examinations including DCE and diffusion-weighted imaging (DWI) were performed on 51 women. The association between kinetic parameters and ADC were evaluated and compared between lesion types. Models with binary outcome of malignancy were studied using generalized estimating equations (GEE),(GEE), and using kinetic parameters and ADC values as malignancy predictors. Model accuracy was assessed using the corrected maximum quasi-likelihood under the independence confidence criterion (QICC). Predicted probability of malignancy was estimated for the best model.

RESULTS: ADC values were significantly associated with kinetic parameters: medium and rapid uptake phase ($p<0.001$) and plateau and washout curve types ($p=0.004$). Comparison between lesion type showed significant differences for ADC ($p=0.001$), early phase ($p<0.001$), and curve type ($p<0.001$). The predicted probabilities of malignancy for the first ADC quartile ($\leq 1.17\times10^{-3}$ mm^2/s) and persistent, plateau and washout curves, were 54.6%, 86.9%, and 97.8%, respectively, and for the third ADC quartile ($\geq 1.51\times10^{-3}$ mm^2/s) were 3.2%, 15.5%, and 54.8%, respectively. The predicted probability of malignancy was less than 5% for 18.8% of the lesions and greater than 33% for 50.7% of the lesions (24/35 lesions, corresponding to a malignancy rate of 68.6%).

CONCLUSION: The best malignancy predictors were low ADCs and washout curves. ADC and kinetic parameters provide differentiated information on the microenvironment of the lesion, with joint models displaying improved predictive performance.

Introduction

Breast magnetic resonance imaging (MRI) is the most sensitive imaging method to detect breast cancer.[1–3] Previous studies have shown its advantages in lesion detection and characterization when compared to mammography and ultrasound.[4–6] Moreover, guidelines and recommendations based on previous single and multicentre studies[7,8] were established for its use in the clinical practice.[3,9–11]

Breast MRI protocols include dynamic contrast-enhanced (DCE) images with high spatial and temporal resolution.[12] Interpretation of those images integrates morphological and kinetic descriptors from the breast imaging report and data system (BIRADS)-MRI lexicon, allowing lesion classification and appropriate recommendations for patient management.[13]

The relevant information regarding DCE lesion kinetics was previously studied.[14–18] The kinetic descriptors rely on tracking the signal intensity (SI) over time, during two phases following a bolus injection of contrast medium: the early phase (wash in) and the delayed phase (washout). Both provide physiological information on lesion vascularity. Kuhl *et al.*[19] reported that the kinetic predictors most associated with malignancy were rapid early enhancement followed by a washout curve in the delayed phase.

A recent meta-analysis by Peters *et al.*[20] including 44 studies, assessed the diagnostic performance of DCE in breast cancer, with an overall sensitivity and specificity of 90% and 72%, respectively. The moderate specificity reflects some overlap in the morphological and kinetic features between benign and malignant lesions, which lead to false-positive cases. The direct consequence of a false-positive diagnosis is that it could result in unnecessary biopsy.

To increase breast MRI specificity, other sources of image contrast should be explored. Diffusion-weighted imaging (DWI) is a promising method. The apparent diffusion coefficient (ADC) quantifies the restriction to the random motion of water molecules within tissues, probing their properties at the cellular level.[21] The ADC is estimated from the SI decay between two or more diffusion-weighting factors (b-values).[22] Increased cellularity restricts the diffusivity of water molecules within tissues, leading to low ADC values.[23] Previous studies have demonstrated the role of DWI in breast lesion detection and characterization.[24–26]

Considering that DWI and DCE kinetics reveal distinct physiological and functional characteristics of the lesion environment, it is likely that combining both may improve lesion characterization. Studies exploring DWI and DCE together have recently been performed,[27–30] suggesting that the specificity and accuracy can be increased. Based on those results, it is important to evaluate the ability of the two combined parameters to predict lesion malignancy. Therefore, the purpose of the present study was to explore the relationship between ADC and kinetic parameters, and to determine their ability to predict malignancy.

Materials and methods

Patients and lesions

A prospective study focusing on breast lesion characterization using DWI-MRI at 3 T was conducted between 2009 and 2012. The study was approved by the Institutional Ethics Committee (protocol: CES 276/13). Women with clinical indications for breast MRI gave their written informed consent.

During 2011, breast MRI examinations were performed in 82 consecutive patients. Clinical indications included unknown primary malignancy, suspicious lesions on mammography and/or ultrasound, preoperative staging, breast cancer screening in women at high-risk, therapeutic monitoring, follow-up after surgery, breast cancer recurrence, and evaluation of implant integrity.

For all pre-menopausal women, breast MRI was performed between the 7th and 14th day of the menstrual cycle to reduce hormonal variations and minimize the enhancement on the fibroglandular tissue.[31,32]

For the purpose of this study, exclusion criteria were applied to patients (1) who had lesions that were biopsied before the MRI examination (n=7); (2) subjected to breast surgery within <6 months (n=6); (3) undergoing radiotherapy and/or chemotherapy within the previous 48 months (n=5); (4) with only simple cystic lesions (n=6); (5) who had completed hormone-replacement therapy within <24 months (n=3); (6) with breast implants (n=1); and (7) whose images had motion artefacts (n=3).

Lesions were included in the analysis if: (1) they were solid; (2) the histological results or a minimum of 2-year follow-up with mammography, ultrasound, or breast MRI were available[33]; (3) their size was ≥7 mm; and (4) they were classified as 3 to 5 in the BIRADS-MRI lexicon and were not biopsy-proven prior to breast MRI examination to exclude the influence of haematoma and/or oedema in the ADC estimates.

Acquisition protocol

All the examinations were performed using a 3 T MRI system (Magnetom® Tim Trio, Siemens Medical Solutions, Erlangen, Germany) using a four-channel phased-array coil

Table 1

Scanning magnetic resonance imaging (MRI) protocol.

Parameters	Conventional pre-contrast			DWI-SPAIR	Dynamic	Post-contrast
Sequence	T2W TSE	T1W 3D FLASH	STIR	Single-shot EPI	T1W 3D FLASH	T1W 3D FLASH
Orientation	Axial Bilateral	Sagittal Unilateral	Sagittal Unilateral	Sagittal Unilateral	Axial Bilateral	Sagittal Unilateral
TR/TE (ms)	4990/88	17/4.9	4920/67	4900/106	3.77/1.42	7.8/3.9
TI (ms)	–	–	210	–	–	–
Fat suppression	–	–	STIR	SPAIR	SPAIR	Water excitation
FOV (mm^2)	320×320	200×200	200×200	250×250	320×320	160×160
Matrix	512×384	275×384	448×314	84×128	358×448	256×256
Section thickness (mm)	4	2	4	5	0.9	0.9
Number of sections	26	64	26	16	160	144
NEX	2	1	2	3	1	1
Bandwidth (Hz/pixel)	305	430	248	1628	490	450
Scan time (min)	2:06	3:49	4:26	5:58	4:32	3:12
b-values (s/mm^2)	–	–	–	50,200,400, 600,800,1000, 2000 and 3000	–	–

DWI-SPAIR, diffusion-weighted imaging with spectrally adiabatic inversion recovery; TSE, turbo spin eco; T1W 3D Flash, T1-weighted three-dimensional gradient echo fast low angle shot; EPI, echo planar imaging; TR/TE, repetition time/echo time; TI, inversion time; STIR, short tau inversion recovery; FOV, field of view; NEX, number of excitations.

(*Invivo*, Corporation, United States) with the patients lying in the prone position. The protocol included conventional MRI and DWI sequences. The sequential order of the acquisitions is presented in Table 1.

Axial dynamic images were acquired, one before and five phases after bolus injection of gadobenate dimeglumine (MultiHance; Bracco, Milan, Italy). Automatic injection was performed via the antecubital vein at a rate of 2 ml/s (total dose 0.1 mmol/kg body weight), followed by a 20 ml saline flush.

The DWI acquisition was performed before DCE. A single-shot spin-echo echo planar imaging (SS-SE-EPI) sequence with eight b-values was used. The diffusion gradients were applied along the *x*-, *y*-, and *z*-directions to generate three-scan-trace images.

To avoid having to estimate the SI for all DWI images and simplify the analysis, only the images with b-values of 50 and 1000 s/mm^2 were used to estimate the ADC. These b-values were chosen according to a previous study aiming to determine the best pair of b-values for breast lesion differentiation.[34] The higher b-values were used to investigate non-Gaussian diffusion of water in lesions.[35]

Including higher b-values (2000 and 3000 s/mm^2) in the protocol resulted in prolonging the echo time (TE) from 78 to 106 ms. As the T2 relaxation time for normal glandular tissue is 71±6 ms,[36] the predicted signal loss from using a longer TE is of 33%. To compensate for this, the number of excitations was increased to 3.

Fig 1 illustrates a case of a 57-year-old woman with a suspicious breast mass located in the upper half of the right breast.

Image analysis

All the datasets were evaluated on the scanner workstation (*Syngo* Multimodality, Siemens Healthcare, Erlangen, Germany) with the commercial software (*Syngo MR* version 17A). The same experienced radiologist (with 6 years of experience in breast MRI) evaluated all the examinations prospectively. Lesion interpretation was based on the BIRADS-MRI lexicon according to morphological and kinetic criteria.[13] For each lesion, the location and size were reported. Lesion size was determined from DCE images and the largest dimension was considered. The morphological features of mass lesions were described (type, shape, margin, and internal enhancement), while for non-mass lesions, the distribution, internal enhancing pattern, and symmetry of enhancement were noted.

The analysis of kinetic parameters was performed on the early T1-weighted subtracted images. For each lesion regions of interest (ROIs) were placed within the area showing the strongest enhancement, and time–SI curves were created. The early phase was measured in the first 1–2 minutes (wash-in rate) after gadolinium injection, and was described as either slow, medium, or rapid. A wash in rate greater than 80% was classified as fast; between 50% and 80% as medium (intermediate); and less than 50% as slow.[12]

After peak enhancement, the delayed phase (washout) corresponding to the remaining time course of the SI curve was classified as having persistent (type I), plateau (type II), and washout (type III) curves. A persistent pattern implies that the SI keeps on increasing during the measurement time; the plateau is typically a curve with constant SI after the early phase. The washout pattern describes the cases for which the SI decreases more than 10% over time, after reaching its highest point in the early phase. Information regarding conventional MRI was based on the clinical MRI report and histopathology results.

The DWI images were analysed by locating the lesions on the conventional MRI images using the information on the clinical report. To measure lesion SI, fixed ROIs of 0.25 cm^2 were drawn firstly at b=1000 s/mm^2, in the section with largest lesion dimension and best definition of its borders, within the area with highest hyperintensity. During ROI demarcation, care was taken to exclude normal fibroglandular tissue, necrotic or cystic areas, and regions with high T2 signal within the lesion. The ROIs were then copied to the b=50 s/mm^2 images. For each lesion, the mean value and standard deviation (SD) of the SI were recorded.

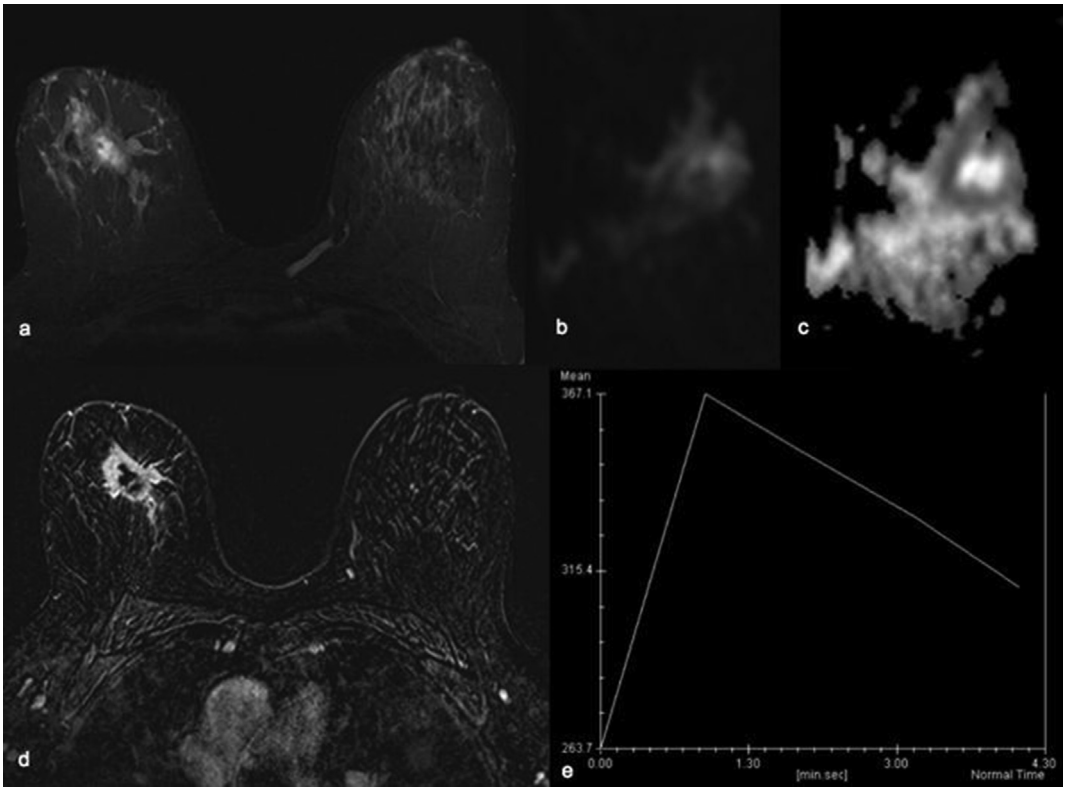

Figure 1 A 57-year-old woman with a suspected malignant lesion in the right breast. (a) Axial short-tau inversion recovery (STIR) shows a large hyperintense lesion with slight hypointense borders. (b) DWI at b=1000 s/mm^2 and (c) the corresponding ADC map. (d) DCE image shows a mass with irregular borders and (e) demonstrating rapid initial contrast enhancement in the early phase followed by washout curve. The histological result revealed an invasive ductal carcinoma grade III, which was in agreement with the ADC value of 0.63×10^{-3} mm^2/s.

The ADC estimate was determined using a linear fitting to the mono-exponential model and two b-values (50 and 1000 s/mm^2) using the equation[21]:

$$\mathrm{ADC} = \frac{\ln[S(b_1)] - \ln[S(b_2)]}{b_2 - b_1}$$

where $S(b)$ represents the signal intensity, and *b1* and *b2* are the two b-values.

Statistical analysis

To characterise the study population, descriptive analysis was performed. The prevalence of lesions characteristics (benign or malignant) was compared using the Pearson chi-squared test (χ^2) and the Fisher's exact test. A one-way ANOVA (analysis of variance) was used to evaluate the association between ADC and kinetic parameters (early-phase and delayed-phase curve). Mean ADC values and kinetic parameters were compared for benign and malignant lesions using the independent sample *t*-test and the Chi-squared test. Models for binary outcome, considering ADC and kinetic parameters as predictors of malignancy, were studied by multilevel regression using the generalized estimating equations (GEE), to account for multiple lesions in the same patient.

The goodness of fit of the models (accuracy) was estimated by the corrected maximum quasi-likelihood under the independence confidence model criterion (QICC): a lower QICC corresponds to a better fit.

Considering curve type and ADC values (quartiles) as predictor variables, the predictive ability for malignancy of the models was calculated. ADC was classified as either lower than the 25% quartile, higher than the 75% quartile, or belonging to the intermediate range.

Table 2
Characteristics of 69 breast lesions and comparison between lesion types.

DCE findings	Malignant (28)		Benign (41)		*p*-Value
	No.	%	No.	%	
Size					0.10
7–10 mm	8	28.6	11	26.9	
11–20 mm	10	35.7	23	56.0	
≥21 mm	10	35.7	7	17.1	
Lesion type					0.31[a]
Mass	22	78.6	36	87.8	
Non-mass	6	21.4	5	12.2	
BI-RADS					<0.001[a]
3	3	10.7	19	46.3	
4	10	35.7	13	31.7	
5	15	53.6	5	12.2	
Diagnostic source					<0.001
Biopsy	28	100.0	30	73.2	
Follow-up	0	0	11	26.8	

[a] Fisher exact test.

All analyses were performed with the PASW version 21.0 and a p-value of less than 0.05 was considered to indicate a statistical significant value.

Results

The final sample included 51 patients (mean age ± SD, 48.4±2.5 years; age range 21–78 years) with 69 lesions detected on both DCE-MRI and DWI. Table 2 presents the characteristics of the lesions and p-values for the comparison between benign and malignant lesions (disregarding sub-groups).

Thirty-seven patients were premenopausal. Among the 69 lesions found, 28 were malignant lesions. Lesion sizes ranged from 7 to 74 mm; there were no significant differences in size between the benign and malignant lesions (p=0.10). Eighty-four percent were mass lesions. Considering the BIRADS classification, 89.3% of the malignant lesions were classified as BIRADS 4 and 5, whereas 56.1% of the benign lesions were classified as BIRADS 3.

Fifty-eight lesions underwent biopsy, from which 28 were classified as malignant. Histopathological results from the malignant lesions included: six ductal carcinoma in situ (DCIS), 13 invasive ductal carcinoma (IDC), four lobular carcinoma in situ (LCIS), three invasive lobular carcinoma (ILC), and two other malignant lesions (NOS). For the 30 benign lesions, histopathological results revealed 14 fibroadenomas (FA), three papillomas, one hamartoma (HA), and 12 classified as other benign lesions, namely 11 cases of fibrocystic change (FC) and one complex sclerosing adenosis (CSA). For the remaining 11 lesions classified as benign, the diagnosis was established by a 2-year follow-up, as recommend by Kopans,[33] which requires imaging

Table 3
Association between apparent diffusion coefficient (ADC) and dynamic contrast-enhanced magnetic resonance imaging (DCE-MRI) kinetic parameters for all lesions (one-way analysis of variance test).

	No. (%)	ADC ($\times 10^{-3}$ mm^2/s) (Mean ± SD)	Association with ADC (p-value)
Early phase			
Slow	2 (2.9)	1.86 ± 0.15	<0.001[a]
Medium	42 (60.9)	1.72 ± 0.46	
Rapid	25 (36.2)	1.24 ± 0.53	
Curve type			
Persistent	21 (30.4)	1.79 ± 0.49	0.004[b]
Plateau	35 (50.7)	1.55 ± 0.50	
Washout	13 (18.8)	1.17 ± 0.52	

[a] Analysis performed only between medium and rapid uptake of gadolinium contrast.
[b] Analysis performed between plateau and washout curve type.

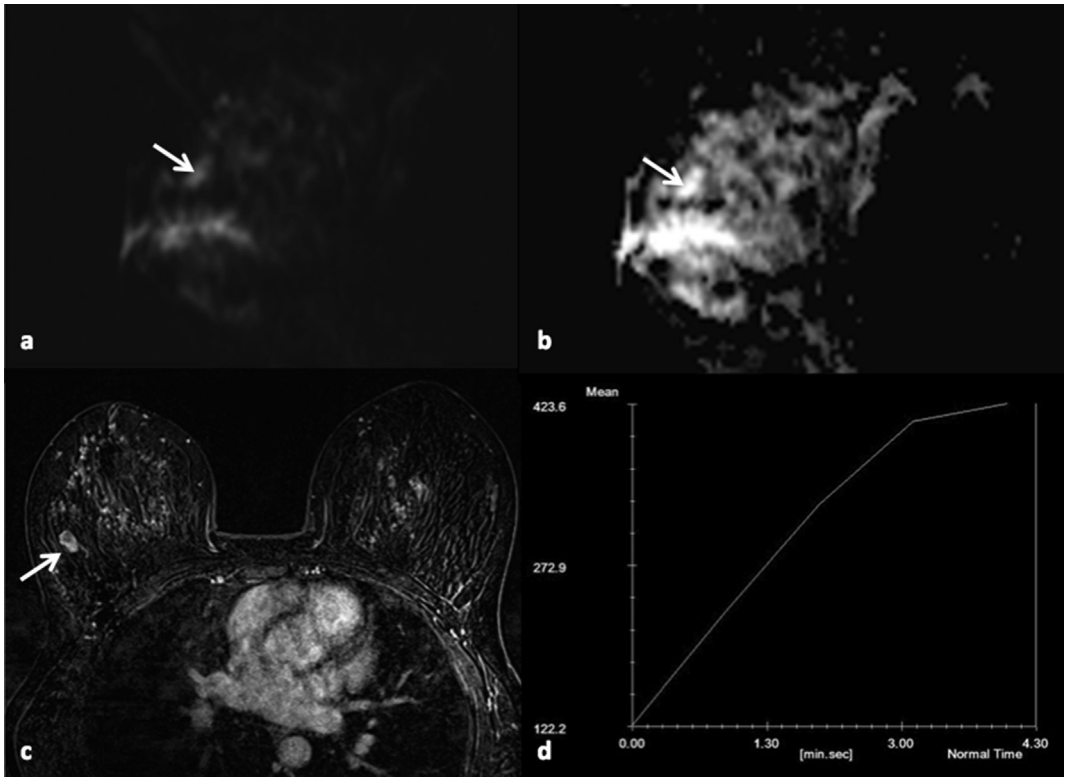

Figure 2 A 34-year-old woman with a suspected mass lesion with 13 mm located in the outer quadrant of the right breast. (a) Sagittal DWI images at b=1000 s/mm^2 revealed a mass lesion with uniform SI and (b) the corresponding ADC map. (c) Axial bilateral DCE image shows a mass with regular borders with (d) slow initial contrast enhancement in the early phase, followed by a persistent curve. Histological result indicated a FA with ADC value of 1.65×10^{-3} mm^2/s.

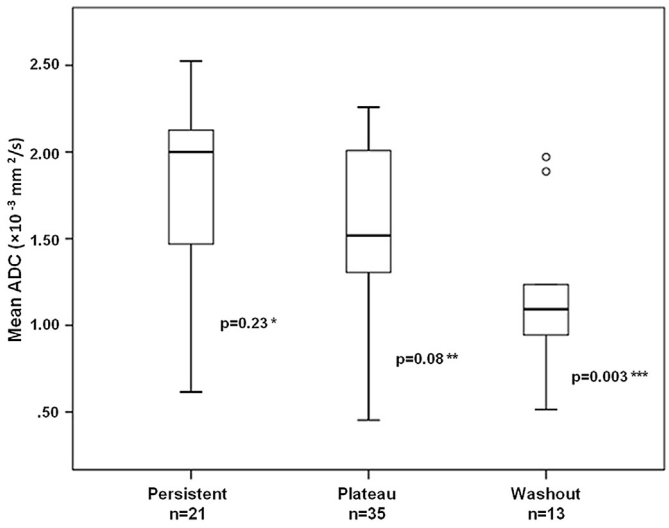

Figure 3 Boxplot of ADC values by curve type. Comparison of ADC values between curve types: persistent/plateau*, plateau/washout**, and washout/persistent***.

Table 4
Univariate comparison between benign and malignant lesions.

	Malignant (28)	Benign (41)	*p*-Value
	Mean ± SD	Mean ± SD	
ADC ($\times 10^{-3}$ mm^2/s)	1.11 ± 0.49	1.74 ± 0.38	<0.001[a]
Early phase			
Slow	0 (0.0%)	2 (4.9%)	<0.001[b]
Medium	9 (32.1%)	33 (80.5%)	
Rapid	19 (67.9%)	6 (14.6%)	
Curve type			
Persistent	0 (0.0%)	21 (51.2%)	<0.001[b]
Plateau	17 (60.7%)	18 (43.9%)	
Washout	11 (39.3%)	2 (4.9%)	

ADC, apparent diffusion coefficient.
[a] Student's *t*-test.
[b] Chi-squared test (χ^2).

stability on mammography, ultrasound, and/or MRI, and included: nine FA, one HA, and one FC. From these lesions, histological results were available prior to this study for two FA and one FC. These lesions were diagnosed in women with BRCA mutation who undergo annual MRI follow-up.

Fig 2 shows a benign lesion in a 34-year-old woman with a suspected breast mass with 13 mm located in the outer quadrant of the right breast.

Association between ADC and DCE-MRI kinetic parameters

The association between ADC values and DCE kinetic parameters were evaluated for all the lesions (Table 3). A significant association was found between ADC values and peak initial enhancement ($p<0.001$). The same was observed between ADC and curve type. Lesions with higher ADC values displayed persistent enhancement more often than washout or plateau enhancement curve patterns ($p=0.004$).

Fig 3 presents ADC distribution by curve type and a comparison of ADC values between curve types. Regarding the pairs of curve types (Bonferroni test) only the pair washout/persistent was significantly different in ADC values ($p=0.003$).

Univariate comparison between ADC and kinetic parameters by lesion type

The results for the comparison between malignant and benign lesions using ADC and DCE kinetics are presented in Table 4. When comparing mean ADC values by lesion type, benign lesions displayed higher ADCs than malignant ones ($1.74\pm0.38\times10^{-3}$ mm^2/s versus $1.11\pm0.49\times10^{-3}$ mm^2/s; $p<0.001$).

The early phase seems to be a good predictor of malignancy ($p<0.001$). In the present study, none of the malignant lesions presented slow gadolinium uptake. Most of the benign lesions (80.5%) showed medium uptake, 14.6% showed rapid, and 4.9% slow uptake. A strong overlap was observed between benign and malignant lesions, especially between medium and rapid uptake.

When the analysis was performed by curve type, malignant lesions showed a higher number of lesions with washout compared to benign ones ($p<0.001$). Seventeen malignant lesions presented a plateau curve (60.7%); 11 (39.3%) had shown washout and none presented a persistent curve.

More than 50% of the benign lesions showed a persistent curve, while the other 43.9% showed a plateau pattern. The remaining 4.9% of the benign lesions, corresponding to two lesions presented washout curves.

Table 5
Generalized linear model (generalized estimating equations, GEE) with binary outcome malignancy using apparent diffusion coefficient (ADC) and curve type patterns as predictor variables.

	Coefficient B	Standard error	Wald	*p*-Value	95% CI
Curve type					
Persistent	−3.603	1.149	9.826	0.002	−5.855; −1.350
Plateau	−1.892	0.760	6.201	0.013	−3.381; −0.403
Washout	–	–	–	–	–
ADC ($\times 10^{-3}$ mm^2/s)	–	–	12.801	0.002	–
1.51–2.53	–	–	–	–	–
1.18–1.50	0.993	0.816	1.481	0.224	−0.606; 2.592
≤1.17	3.593	1.047	11.785	0.001	1.542; 5.645

95% CI, 95% confidence interval.

Table 6
Probability of malignancy for apparent diffusion coefficient (ADC) quartiles and the curve type.

ADC Quartile	ADC range ($\times 10^{-3}$ mm^2/s)	Curve type					
		Persistent		Plateau		Washout	
		No.	Probability of malignancy (%)	No.	Probability of malignancy (%)	No.	Probability of malignancy (%)
1° Q – 25%	≤1.17	2	54.6	7	86.9	8	97.8
2° Q – 50%	1.18–1.50	6	8.2	9	33.1	2	76.6
3° Q – 75%	≥1.51	13	3.2	19	15.5	3	54.8

Multivariate analysis for lesion discrimination

A GEE analysis was performed considering: the ADC values (classified based on quartile measurements to guarantee that each category included at least 25% of the lesions), the early phase, and curve type as predictors of malignancy. According to the criterion of the lowest QICC (the corrected quasi-likelihood under independence model criterion), the model that best predicted lesion malignancy included both ADC value and curve type (QICC=56.931). When the early phase was added to the model, the QICC was worse (QICC=58.165), and the effect of this parameter was not found to be significant (p=0.311). When only the ADC values were used to predict malignancy, the QICC was even higher (61.068), indicating that complementary information is indeed provided by the curve type parameter. Table 5 presents the final results of the best model. Based on the results of the GEE model with outcome malignancy and independence working correlation, ADC and curve type were independent predictors of malignancy (p=0.003 and p=0.004, respectively). The predicted probabilities of malignancy based on the multivariable GEE model are summarized in Table 6.

The predicted probabilities of malignancy for the first ADC quartile corresponding to 25th percentile ($\leq 1.17\times10^{-3}$ mm^2/s) were 54.6% for persistent, 86.9% for plateau, and 97.8% for washout curve, respectively. For the second ADC quartile ($1.18-1.50\times10^{-3}$ mm^2/s) the probabilities of malignancy for persistent, plateau, and washout curve types were 8.2%, 33.1%, and 76.6%, respectively. For the third ADC quartile, corresponding to 75th percentile ($\geq 1.51\times10^{-3}$ mm^2/s), the predicted probabilities of malignancy were only 3.2% for persistent, 15.5% for plateau, but more than 54.8% for a washout curve.

From the 69 lesions, 18.8% had a predicted probability of malignancy <5% (with one malignant among 28 lesions) and 50.7% had a predicted probability of malignancy >33% (with 24/35 lesions, corresponding to a malignancy rate of 68.6%). Fig 4 illustrates an atypical cancer case corresponding to an invasive lobular carcinoma classified as grade II with strong initial enhancement followed by a plateau curve type.

Discussion

Breast cancer is one of the main public health problems worldwide.[37] As an adjunct tool to mammography and ultrasound, breast MRI is increasingly used, mostly due to its high sensitivity to detect and characterise early invasive breast cancer.[38]

Previous studies on DCE-MRI[8,15] reported kinetic parameters as having high diagnostic value and the washout curve as a strong discriminator for lesion malignancy.[27] DCE images provide information about the rate of tissue enhancement followed by the rate of contrast washout, reflecting tissue vascularity, vessel permeability, and diffusion in the extra-vascular space.[12,39] Based on differences in temporal enhancement, it is possible to distinguish benign from malignant lesions. Also, previous studies reported that DWI is useful in the differentiation between benign and malignant breast lesions.[23,24] DWI provides functional information at the cellular level.[40] Pathological processes result in increased cellularity and structural changes, leading to a more compact tissue with reduced extracellular space and water mobility.[23] The ADC measures that restriction, serving as an indirect index of tissue complexity. Recent studies reported that a protocol with both DCE and DWI improves diagnostic performance and accuracy.[27–30] Therefore, the physiological (kinetic parameters) and functional (ADC) information derived from both techniques can be used to predict malignancy.

In the present study, the mean ADC values of malignant lesions were significantly lower than benign ones (mean ADC values for malignant lesions were $1.11\pm0.49\times10^{-3}$ mm^2/s and for benign $1.74\pm0.38\times10^{-3}$ mm^2/s), in the range of the mean ADCs published by other groups.[41,42]

The association found between ADC and kinetic parameters indicates that both can contribute to lesion characterization. In the present study, the higher mean ADC values were associated with persistent enhancement and the lower ADCs with lesions with rapid enhancement and plateau/washout patterns. A previous study reported that these kinetic characteristics are frequently associated with lesions suspicious of malignancy.[27] Also, Partridge *et al.*[43] studied the relationship between DCE kinetic features and ADCs, and they found a significant association only between the ADC and the curve type. In the present study, a significant association was found between the ADC and both kinetic parameters. Although there are differences in the analysis of the early phase, as the authors of that study measured SI variation along the early phase of the DCE,[43] the most probable explanation is the nature of the neoangiogenesis of the lesions was different in the present study.

Comparison between benign and malignant lesions showed that the ADC value, early phase, and curve type are strong predictors for lesion discrimination; however, a

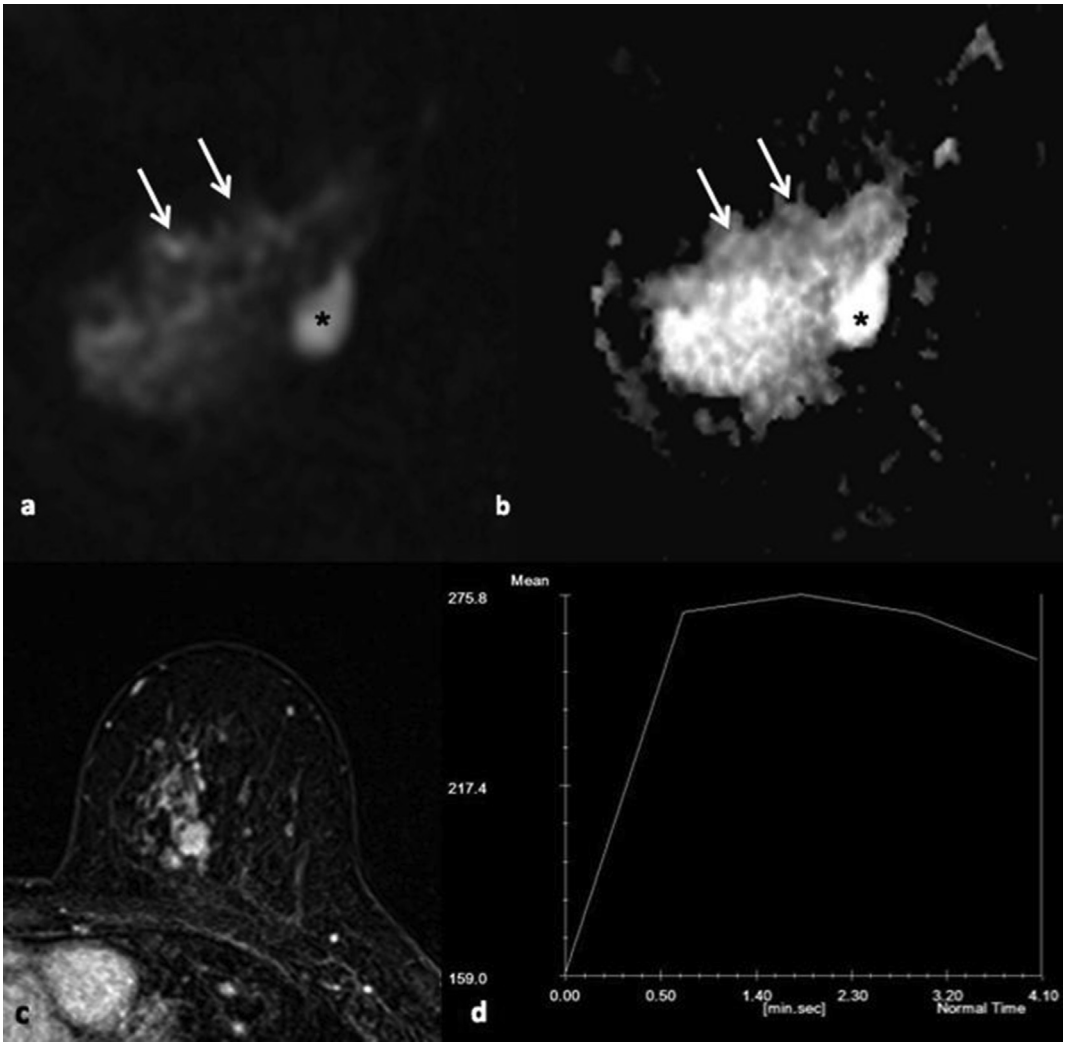

Figure 4 A 50-year-old woman with a suspected mass lesion with 11 mm located in the transition of the superior quadrants of the left breast. (a) Sagittal DWI image at b=1000 s/mm^2 revealed an isohyperintense mass lesion (arrows), and (b) the corresponding hypointensity in the ADC map (arrows). Image (c) is an early-phase subtraction of the DCE sequence. The lesion presents irregular borders and heterogeneous signal intensity. (d) The kinetic curve shows strong contrast enhancement in the early phase, followed by a plateau curve. The histological result showed an invasive lobular carcinoma with an ADC value of 1.36×10^{-3} mm^2/s. The asterisks on (a) and (b) illustrate a simple cyst with high signal on both b=1000 s/mm^2 and ADC map because of the long T2 relaxation time of the fluid (T2 shine-through).

strong overlap was observed in the early phase, with malignant lesions showing medium and benign lesions depicting rapid uptake of gadolinium.

Although malignant lesions more often displayed a washout pattern when compared to benign lesions, two benign lesions presented a washout pattern and low ADC values, namely one FA and one FC. The most probable explanation is that these lesions, presenting high cellularity due to increased proliferation, also show increased neovascularisation activity.

A strong overlap in the plateau pattern and ADC values was also found for benign and malignant lesions. Some malignant lesions presented plateau curves and higher ADC, namely two DCIS and two ILC lesions, and benign lesions presenting a plateau pattern and lower ADC values (one FC and one CSA). This overlap in kinetic imaging features and ADCs values had already been reported by other groups[44,45] and is related to the wide spectrum of breast lesion heterogeneity, even within the same histological type.

Multivariate analysis revealed that the model that best predicted lesion malignancy incorporates information regarding both ADC and curve type. Lower ADC values and plateau or washout curves were the best predictors of malignancy. A previous study developed by Yabuuchi *et al.*[27] used correlation to evaluate the diagnostic accuracy of several discriminators for benign versus malignant enhancing mass lesions using the same pulse sequences as the present work. The authors found some morphological characteristics, plateau and washout curves and ADC values, to be the strongest discriminators between benign and malignant lesions. In the present study, the predicted probabilities of malignancy were higher when a washout pattern is present and the ADC is $\leq 1.17\times10^{-3}$ mm^2/s. Using the ADC and curve type as predictors, the malignancy rate

was 68.6%, with 19 from the 28 malignant lesions correctly classified. Based on the stratification of ADC and curve type, malignancy prediction could be useful in the clinical setting to reduce the number of unnecessary biopsies, thus improving lesion management.

In the present work the focus was the physiological information retrieved from DCE-MRI. Although morphological features (type, shape, margin, distribution, and internal enhancement pattern) were not used to predict malignancy, the inclusion of those features could further improve the predictive probability of the model.

Although in the authors' breast unit the reference standard for suspicious lesion management is to perform biopsy before the MRI examination, for the present study patients who had previously undergone biopsy were excluded to minimize the presence of haematoma and/or oedema, as these would have influenced the ADC estimates. If oedema is present, an increased in the ADC is expected as the extra fluid reduces the density of barriers hindering the motion of water molecules. The presence of haematoma leads to a reduction in $T2^*$ due to the iron in the lesion, reducing the signal and thus making ADC estimates less reliable.

The present study had some limitations. Firstly, nine lesions were classified based only on the stability of imaging features upon follow-up. Secondly, the number of benign lesions was higher than the malignant ones, introducing some bias in the predictive model of malignancy towards benign lesions.

In conclusion, the information derived from DCE and ADC reflects different information on lesion characteristics. The combination of both examinations could be used in the clinical practice to estimate the predictive value of lesion malignancy. A future study with a larger sample could enhance the predictive value of malignancy.

References

1. Kuhl C. Current status of breast MR imaging. Part 2. Clinical applications. *Radiology* 2007;**244**:672–91.
2. Warner F, Messersmith H, Causer P, et al. Systematic review: using magnetic resonance imaging to screen women at high risk for breast cancer. *Ann Intern Med* 2008;**148**:671–9.
3. Lee CH, Dershaw DD, Kopans D, et al. Breast Cancer Screening with imaging: recommendations from the Society of Breast Imaging and the ACR on the use of mammography, breast MRI, breast ultrasound, and other technologies for the detection of clinically occult breast cancer. *J Am Coll Radiol* 2010;**7**:18–27.
4. Sardanelli F, Giuseppetti G, Panizza P, et al. Sensitivity of MRI versus mammography for detecting foci of multifocal, multicentric breast cancer in fatty and dense breasts using the whole-breast pathologic examination as a gold standard. *AJR Am J Roentgenol* 2004;**183**:1149–57.
5. Kuhl CK, Schrading S, Leutner CC, et al. Mammography, breast ultrasound, and magnetic resonance imaging for surveillance of women at high familial risk for breast cancer. *J Clin Oncol* 2005;**23**:8469–76.
6. Benndorf M, Baltzer PA, Vag T, et al. Breast MRI as an adjunct to mammography: does it really suffer from low specificity? A retrospective analysis stratified by mammographic BI-RADS classes. *Acta Radiol* 2010;**51**:715–21.
7. Leach MO, Boggis CR, Dixon AK, et al. Screening with magnetic resonance imaging and mammography of UK population at high familial risk of breast cancer: a prospective multicentre cohort study (MARIBS). *Lancet* 2005;**365**:1769–78.
8. Schnall MD, Blume J, Bluemke D, et al. Diagnostic architectural and dynamic features at breast MR imaging: multicenter study. *Radiology* 2006;**238**:42–53.
9. Mann R, Kuhl C, Kinkel K, et al. Breast MRI: guidelines from the European Society of breast imaging. *Eur Radiol* 2008;**18**:1307–18.
10. Sardanelli F, Boetes C, Borisch B, et al. Magnetic resonance imaging of the breast: recommendations from the EUSOMA working group. *Eur J Cancer* 2010;**46**:1296–316.
11. American College of Radiology (ACR). *ACR Practice Guideline for the performance of Contrast-enhanced Magnetic Resonance Imaging (MRI) of the breast.* 2013. Available at: http://www.acr.org/~/media/ACR/Documents/PGTS/guidelines/MRI_Breast.pdf [accessed 15.06.14].
12. Kuhl C. The current status of breast MR imaging. Part I. Choice of technique, image interpretation, diagnostic accuracy, and transfer to clinical practice. *Radiology* 2007;**244**:356–78.
13. American College of Radiology (ACR). *Breast imaging reporting and data system atlas (BI-RADS® Atlas).* Reston VA: American College of Radiology; 2003.
14. Kuhl CK, Schild HH, Morakkabati N. Dynamic bilateral contrast-enhanced MR imaging of the breast: trade-off between spatial and temporal resolution. *Radiology* 2005;**236**:789–800.
15. Yabuuchi H, Kuroiwa T, Kusumoto C, et al. Incidentally detected lesions on contrast-enhanced MR imaging in candidates for breast conserving therapy: correlation between MR findings and histological diagnosis. *J Magn Reson Imaging* 2006;**23**:486–92.
16. Merckel LG, Verkooijen HM, Peters NG, et al. The added diagnostic value of dynamic contrast-enhanced MRI at 3.0T in nonpalpable breast lesions. *Plos One* 2014;**9**:e94233.
17. El Khouli RH, Macura KJ, Kamel IR, et al. 3-T dynamic contrast-enhanced MRI of the breast: pharmacokinetic parameters versus conventional kinetic curve analysis. *AJR Am J Roentgenol* 2011;**197**:1498–505.
18. Pinker-Domenig K, Bogner W, Gruber S, et al. High resolution MRI of the breast at 3T: which BI-RADS descriptors are most strongly associated with the diagnosis of breast cancer? *Eur Radiol* 2012;**22**:322–30.
19. Kuhl CK, Mielcareck P, Klaschik S, et al. Dynamic breast MR Imaging: are signal intensity time course data useful for differential diagnosis of enhancing lesions? *Radiology* 1999;**211**:101–10.
20. Peters NH, Borel Rinkes IH, Zuithoff NP, et al. Meta-analysis of MR imaging in the diagnosis of breast lesions. *Radiology* 2008;**246**:116–24.
21. Koh DM, Collins DJ. Diffusion-weighted MRI in the body: applications and challenges in oncology. *AJR Am J Roentgenol* 2007;**188**:1622–35.
22. Roth Y, Ocherashvilli A, Daniels D, et al. Quantification of water compartmentation in cell suspensions by diffusion-weighted and T2-weighted MRI. *Magn Reson Imaging* 2008;**26**:88–102.
23. Pereira F, Martins G, Oliveira R. Diffusion magnetic resonance imaging of the breast. *Magn Reson Imaging Clin N Am* 2011;**19**:95–110.
24. Guo Y, Cai YQ, Cai ZL, et al. Differentiation of clinically benign and malignant breast lesions using diffusion-weighted Imaging. *J Magn Reson Imaging* 2002;**16**:172–8.
25. Woodhams R, Matsunaga K, Kan S, et al. ADC mapping of benign and malignant breast tumors. *Magn Reson Med Sci* 2005;**4**:35–42.
26. Costantini M, Belli P, Rinaldi P, et al. Diffusion-weighted imaging in breast cancer: relationship between apparent diffusion coefficient and tumour aggressiveness. *Clin Radiol* 2010;**65**:1005–12.
27. Yabuuchi H, Matsuo Y, Okafuji T, et al. Enhanced mass on contrast-enhanced breast MR imaging: lesion characterization using combination of dynamic contrast-enhanced and diffusion-weighted MR images. *J Magn Reson Imag* 2008;**28**:1157–65.
28. El Khouli R, Jacobs AM, Mezban DS, et al. Diffusion-weighted imaging improves the diagnostic accuracy of conventional 3.0-T breast MR imaging. *Radiology* 2010;**256**:64–73.
29. Partridge SC, DeMartini WB, Kurland BF, et al. Quantitative diffusion-weighted imaging an adjunct to conventional breast MRI for improved positive predictive value. *AJR Am J Roentgenol* 2009;**193**:1716–22.
30. Kul S, Cansu A, Alhan E, et al. Contribution of diffusion-weighted imaging to dynamic contrast-enhanced MRI in the characterization of breast tumors. *AJR Am J Roentgenol* 2011;**196**:210–7.
31. Partridge SC, McKinnon GC, Henry RG, et al. Menstrual cycle variation of apparent diffusion coefficients measured in the normal breast using MRI. *J Magn Reson Imaging* 2001;**14**:433–8.
32. O'Flynn EA, Morgan VA, Giles SL, et al. Diffusion weighted imaging of the normal breast: reproducibility of apparent diffusion coefficient measurements and variation with menstrual cycle and menopausal status. *Eur Radiol* 2012;**22**:1512–8.
33. Kopans DB. Caution on core. *Radiology* 1994;**193**:325–8.
34. Nogueira L, Brandão S, Matos E, et al. Diffusion-weighted imaging: determination of the best pair of b-values to discriminate breast lesions. *Br J Radiol* 2014;**87**:20130807.
35. Nogueira L, Brandão S, Matos E, et al. Application of the diffusion kurtosis model for the study of breast lesions. *Eur Radiol* 2014. http://dx.doi.org/10.1007/s00330-014-3146-5.
36. Edden R, Smith S, Barker P. Longitudinal and multi-echo transverse relaxation times of normal breast tissue at 3 Tesla. *J Magn Reson Imaging* 2010;**32**:982–7.
37. Ferlay J, Shin HR, Bray F, et al. *GLOBOCAN 2008, Cancer Incidence and Mortality Worldwide: IARC Cancer Base No. 10*. International Agency for Research on Cancer; 2010. Available at: http://globocan.iarc.fr [accessed 15.06.14].
38. Petralia G, Bonello L, Priolo F, et al. Breast MR with special focus on DW-MRI and DCE-MRI. *Cancer Imaging* 2011;**11**:76–90.
39. Warner E, Plewes DB, Shumak RS, et al. Comparison of breast magnetic resonance imaging, mammography, and ultrasound for surveillance of women at high risk for hereditary breast cancer. *J Cin Oncol* 2001;**19**:3524–31.
40. Le Bihan DL, Mangin JF, Poupon C, et al. Diffusion tensor imaging: concepts and applications. *J Magn Reson Imaging* 2001;**13**:534–46.
41. Lo GG, Ai V, Chan JK, et al. Diffusion-weighted magnetic resonance imaging of breast lesions: first experiences at 3 T. *J Comput Assist Tomogr* 2009;**33**:63–9.
42. Iacconi C. Diffusion and perfusion of the breast. *Eur J Radiol* 2010;**76**:386–90.
43. Partridge SC, Rahbar H, Murthy R, et al. Improved diagnosis accuracy of breast MRI through combined apparent diffusion coefficients and dynamic contrast-enhanced kinetics. *Magn Reson Med* 2011;**65**:1759–67.
44. Belli P, Costantini M, Bufi E, Magistrelli A, La Torre G, Bonomo L. Diffusion-weighted imaging in breast lesion evaluation. *Radiol Med* 2010;**115**:51–69.
45. Yabuuchi H, Matsuo Y, Kamitani T, et al. Non-mass-like enhancement on contrast-enhanced breast MR imaging: lesion characterization using combination of dynamic contrast-enhanced and diffusion-weighted MR images. *Eur J Radiol* 2010;**75**:126–32.